# Application of the impedance model of de Levie for the characterization of porous electrodes

**O. E. Barcia, E. D'Elia, I. Frateur, O. R. Mattos, N. Pébère and B. Tribollet**

Universidade Federal de Rio de Janeiro, Rio de Janeiro, Brazil
Lab. de Physico-Chimie des Surfaces, UMR7045 du CNRS, ENSCP, 11 rue Pierre et Marie Curie, 75005 Paris, France
UMR CNRS 5085, ENSIACET, 31077 Toulouse, France
UPR 15 du CNRS, Université Paris 6, 75005 Paris, France

## Abstract

From the de Levie's theory for a porous electrode, the impedance can be expressed in function of the cylindrical pore characteristics: the pore length, the pore radius and the number of pores. If the pores have a finite length, these parameters can be regressed from the experimental impedance diagrams. In the case of a semi-infinite pore length, only the product $r^{3/2}n$ can be obtained. In this paper, two practical examples of porous electrodes were presented: the corrosion of cast iron in drinking water and the electrodissolution of copper in 1 M hydrochloric acid solution. In each case, the pore parameters were assessed.

**Author Keywords:** Porous electrode; Pore parameters; EIS; Cast iron; Copper; Regression procedure

# 1. Introduction

It is very common in the literature to analyze impedance results by a physical model; this model is expressed by a mathematical equation and this equation can be represented by an equivalent circuit. The values of the electrical components of the circuit are associated with the physical/chemical properties of the metal–electrolyte interface. However, in general, experimental impedance is not a semi circle and some dispersion in frequency is normally found. In this case, the so-called constant phase element (CPE) approach is used [1] but it is not always easy to attribute a physical meaning to the regressed parameters, even if a very good fit can be obtained.

A classical example of dispersion in frequency presenting a clear physical meaning was described by de Levie [2] for porous electrodes. He considered that the impedance of a porous electrode could be described by a parallel schema of identical cylindrical pores. The impedance of each pore $Z_{\text{deLevie}}$ was calculated by the transmission line technique, with the following assumptions:

the solution resistivity is independent of the coordinate along the pore axis *x*,

the conductivity of the solid phase is infinite (metallic electrode behavior),

the local impedance is independent of *x*.

Thus no axial concentration gradient is considered and the ohmic drop is neglected.

$Z_{\text{deLevie}}$ (in Ω) is given by:

$$Z_{\text{deLevie}} = (R_0 Z_0)^{1/2} \coth\left(l\sqrt{\frac{R_0}{Z_0}}\right) \quad (1)$$

$R_0$ is the electrolyte resistance for a one-unit length pore in Ω $\text{cm}^{-1}$, $Z_0$ is the interfacial impedance for a one-unit length pore in Ω cm and $l$ is the length of each pore in cm. $R_0$ and $Z_0$ can be expressed in function of the pore radius r as follows:

$$R_0 = \frac{\rho}{\pi r^2} \quad (2)$$

$$Z_0 = Z_{eq}/2\pi r \quad (3)$$

where $Z_{eq}$ is the interfacial impedance per surface unit (in Ω cm$^2$) and $\rho$ the electrolyte resistivity (in Ω cm).

The experimental impedance of a porous electrode $Z_{exp}$ (in Ω) can be written by:

$$Z_{exp} = \frac{Z_{deLevie}}{n} \quad (4)$$

*n* being the number of pores. The combination of (1), (2), (3) and (4) yields an expression of $Z_{exp}$ in function of the three geometrical parameters ł, *r* and *n*:

$$Z_{exp} = \frac{(\rho Z_{eq})^{1/2}}{\sqrt{2}\pi n r^{3/2}} \coth\left(l\sqrt{\frac{2\rho}{rZ_{eq}}}\right) \quad (5)$$

An equivalent equation was previously given by Los et al. [3] for a pure charge transfer-controlled process.

When $l\sqrt{2\rho/rZ_{eq}}$ is large enough, which means that the pores behave as though they are semi-infinitely deep, $\coth\left(l\sqrt{2\rho/rZ_{eq}}\right)$ tends towards 1 and $Z_{exp}$ tends towards $(\rho Z_{eq})^{1/2}/\sqrt{2}\pi n r^{3/2}$. In this particular case, *r* and *n* cannot be determined separately; only the product ($r^{3/2}n$) can be obtained.

When $l\sqrt{2\rho/rZ_{eq}}$ is small enough, $\coth\left(l\sqrt{2\rho/rZ_{eq}}\right)$ tends towards $\left(l\sqrt{2\rho/rZ_{eq}}\right)^{-1}$ and $Z_{exp}$ towards $Z_{eq}/2\pi nlr$. In this case, the impedance corresponds to that of a plane electrode.

When $l\sqrt{2\rho/rZ_{eq}}$ has an intermediate value, $\coth\left(l\sqrt{2\rho/rZ_{eq}}\right)$ differs from 1 and the geometrical parameters ł, *r* and *n* can be regressed from the experimental data.

Different pore geometries were taken into account by several authors. Keiser et al. [4] calculated in 1976 the impedance of occluded pores of finite depth by numerical simulation. They only considered the case where $Z_0$ was purely capacitive due to the double layer capacitance. In 1981, Candy et al. [5] reported the impedance of porous electrodes made of gold-powder and Raney-gold. It was shown that even for a very intricate pore-form, the overall impedance was equivalent to that of a cylindrical pore electrode with equivalent pore length, pore radius and number of pores. This approach was also used to characterize the pore

texture of Raney-nickel [6]. More recently, numerical simulations of impedance data for different pore geometries were carried out by Hitz and Lasia [7]: pear-shape, spherical and two spheres pore shapes were considered.

Because the pores are distributed (various dimensions), the use of a one pore model to describe the electrode surface only provides average values for the pore parameters. A model taking into account distribution of simple cylindrical pores was recently published by Song et al. [8].

In order to obtain an analytical solution, de Levie assumed that the interfacial impedance was independent of the distance within the pore ($x$), which means that the ohmic drop along the pore as well as the axial concentration gradient are negligible. Impedance of porous electrodes in the presence of a concentration gradient was studied numerically by Keddam et al. [9] and Cachet and Wiart [10] but the ohmic drop in the pores was neglected. In 1995, a model for porous electrodes, assuming Butler–Volmer equation at the pore interface, was presented by Lasia who took into account the ohmic drop but not the concentration gradient [11]. In the case of finite-length cylindrical pores, he obtained only numerical solutions. A complete numerical calculation in the presence of a concentration gradient and a potential drop in the pores was developed later by the same author [12].

The aim of the present paper is to fit experimental impedance data of systems that exhibit a porous behavior. For this purpose, an analytical porous electrode model is much more convenient than a numerical one. Thus, in the absence of information on the pore geometry, cylindrical pores will be considered and the de Levie's theory used. Two practical examples will be presented: the corrosion of cast iron in drinking water and the electrodissolution of copper in 1 M hydrochloric acid solution. In each case, mean values for the geometrical pore parameters will be obtained and the corresponding assumptions of de Levie's model will be discussed.

## 2. Corrosion of cast iron in drinking water

Free chlorine (Cl; the sum of hypochlorous acid HOCl and hypochlorite ions $ClO^-$) introduced in drinking water in order to maintain microbiological quality, gradually disappears throughout distribution networks. The corrosion of cast iron pipes, which represent around 70% of the French networks, has been recently invoked as an important source of

chlorine decay [13]. Indeed, CL is chemically reduced by ferrous ions released by the metal dissolution [14].

## 2.1. Experimental

All electrochemical measurements were performed with a three-electrode cell. The working electrode was a cast iron rotating disk electrode (RDE) of 5 mm diameter, directly machined from a typical pipe. Its rotation speed was fixed to 150 rpm. The counter electrode was a large platinum grid, and potentials were referred to a saturated sulfate electrode (SSE). The electrolyte was commercial Evian mineral water, used as delivered. Experiments were carried out either without CL, in a single compartment cell, or with CL, in a two-compartment cell. Free chlorine was added to water as bleach. Its concentration was fixed to 0.5 or 2 mg $l^{-1}$. More details about the experimental conditions are given elsewhere [15].

Ac impedance diagrams were collected by means of a 1287 SOLARTRON potentiostat–galvanostat and a 1250 SOLARTRON Frequency Response Analyzer with a frequency domain ranging from 60 kHz to a few mHz.

## 2.2. Experimental impedance diagrams

In Fig. 1, impedance diagrams are plotted at different times of immersion with 2 mg $l^{-1}$ of CL. All diagrams show qualitatively the same features. They can be described by two capacitive loops, a high-frequency (HF) loop to which corresponds a very small capacitance value, much lower than the usual double layer capacitance, and a low-frequency (LF) loop which has the appearance of a diffusion impedance. During the first days of immersion, the high-frequency part of the diffusion impedance exhibits an angle of 45° with respect to the real axis, the same as observed for a plane electrode. This angle approaches gradually 22.5° for increasing immersion times, which suggests that the cast iron electrode behaves as a semi-infinite porous medium, in agreement with the theory of de Levie [2].

Fig. 1. (●) Experimental and (□) regressed ac impedance diagrams of the cast iron RDE, plotted at $E_{corr}$ and 150 rpm, in function of immersion time in Evian mineral water added with 2 mg $l^{-1}$ of CL. Some frequencies expressed in Hz are indicated on the diagrams.

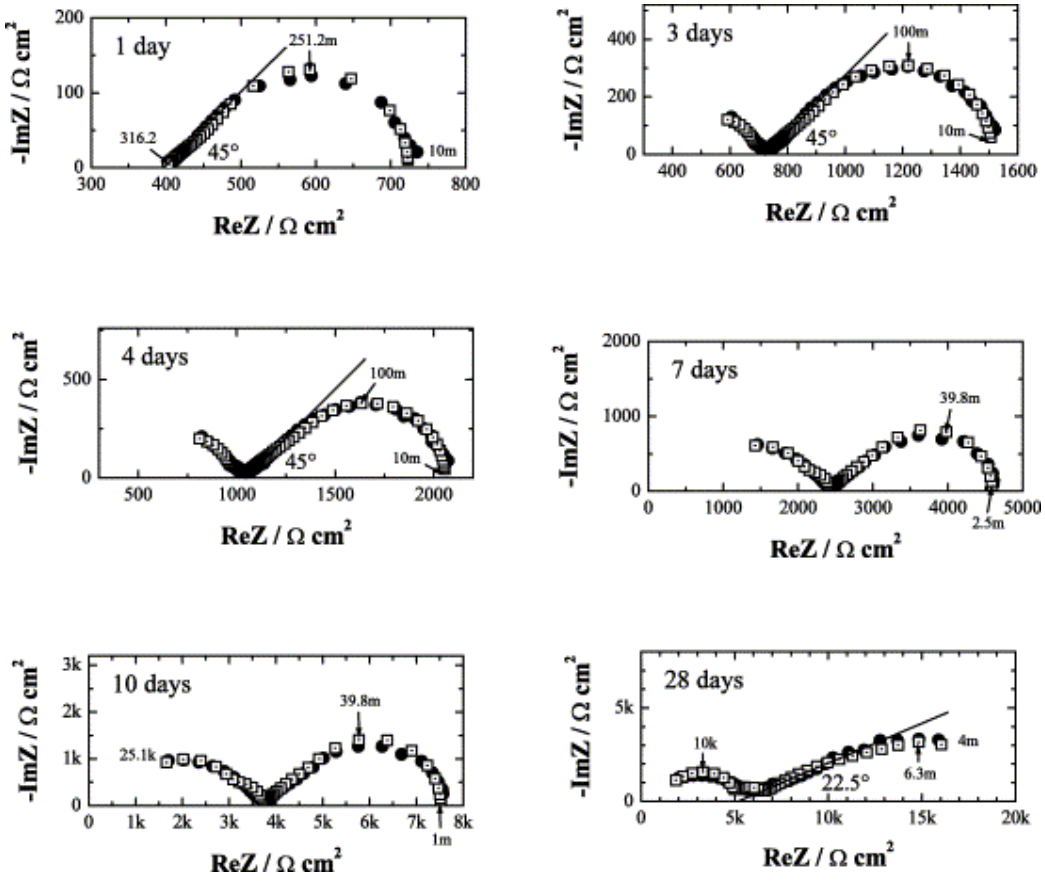


In the absence of CL, both loops are very flattened, even at short times (angle of 22.5° from the first day of immersion) [15]. Moreover, the comparison of results obtained with 0.5 and 2 mg $l^{-1}$ of CL shows that for any time of immersion, a variation of CL concentration does not modify the overall shape of the impedance diagrams. Therefore, the electrochemical response of cast iron depends only on the presence or the absence of CL and not on its concentration.

The porous electrode behavior detected on impedance diagrams is confirmed by optical observations that show a porous black rust layer but the geometrical characteristics of the pores cannot be assessed due to the presence of a top red rust layer.

As it will be shown further, the corrosion study of cast iron in drinking water is an example where the use of the de Levie's theory is the only way to get a good adjustment of impedance data.

## 2.3. Physical model

The scheme proposed for the cast iron–drinking water interface is illustrated in Fig. 2 [15]. From this physical model, an electrical model of the interface can be given ( Fig. 3). This latter model, that takes into account the porous electrode model of de Levie [2], describes the behavior of cast iron in drinking water, with and without free chlorine, and at any time of immersion.

Fig. 2. Physical model of the cast iron–drinking water interface. Equivalent circuit for the cathodic impedance.

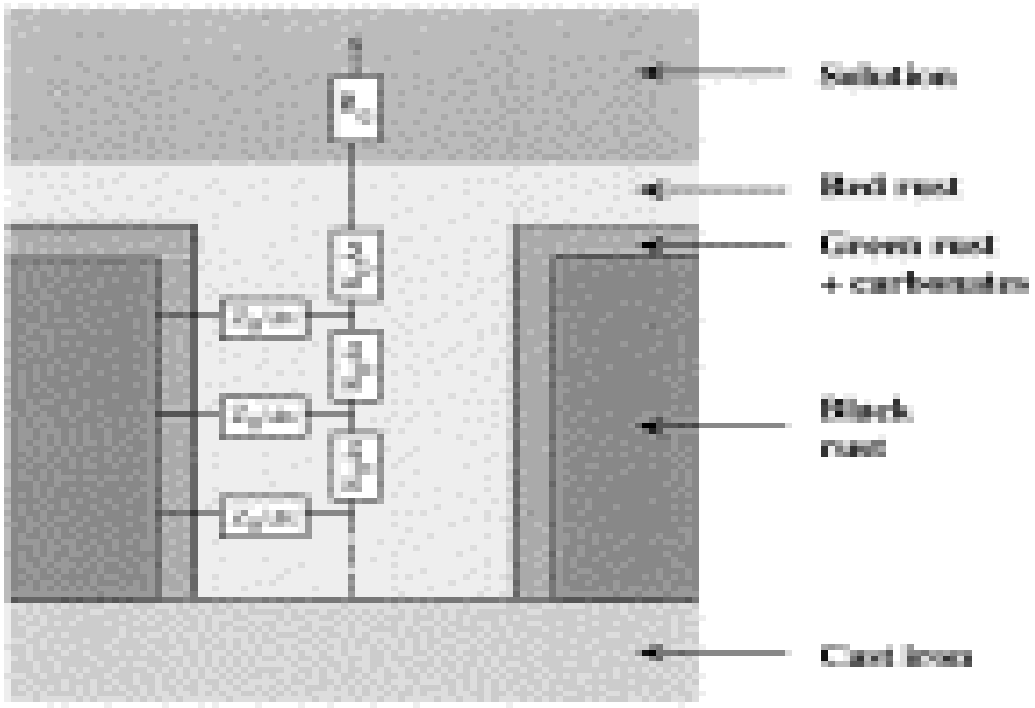

Fig. 3. Electrical model for the cast iron–drinking water system, at $E_{corr}$. Equivalent circuit for (a) the total impedance, (b) the anodic impedance and (c) the interfacial impedance for a one-unit length macropore $Z_0$.

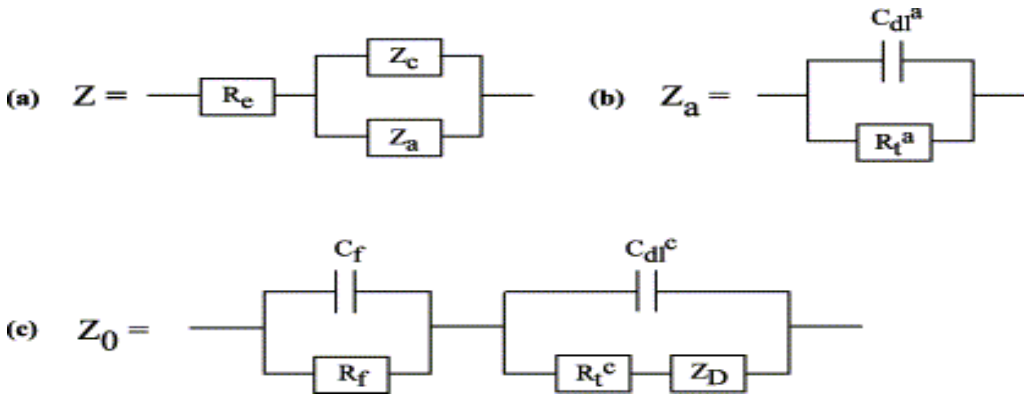


Near the corrosion potential, the total impedance is equivalent to an anodic impedance $Z_a$ linked in parallel with a cathodic impedance $Z_c$, with the solution resistance $R_e$ added in series (Figs. 3(a) and (b)). With the previous notation the cathodic impedance $Z_c$ corresponds to $Z_{deLevie}/n$. $Z_0$ which is seen through the micropores, is composed of the parallel arrangement $R_f/C_f$ ($R_f$ is the ohmic drop resistance of the electrolyte through the microporous film and $C_f$ the film capacitance) in series with the parallel arrangement of the cathodic double layer capacitance $C_{dl}^c$ and the Faradaic branch consisting of a cathodic charge transfer resistance $R_t^c$ in series with a diffusion impedance $Z_D$ (Fig. 3(c)).

$Z_D$ which describes the radial diffusion (relatively to the macropores) of oxygen through the green rust layer is given by [16]:

$$Z_D = R_D \frac{th\sqrt{j\omega\tau_D}}{\sqrt{j\omega\tau_D}} \tag{6}$$

with

$$\tau_D = \frac{\delta_r^2}{D_r} \tag{7}$$

where $R_D$ is the diffusion resistance, $\tau_D$ the diffusion time constant, $\delta_r$ the thickness of the diffusion layer that equals the thickness of the green rust layer and $D_r$ is the diffusion coefficient of dissolved oxygen in this layer.

Thus the anodic surface corresponds to the end of the macropores whereas the cathodic reaction occurs at the end of the micropores. Moreover, it should be noted that $l$, $r$ and $n$ are relative to the macropores.

Given the very low value of the corrosion current, the axial ohmic drop is negligible. As the diffusion of dissolved oxygen occurs only through the green rust layer, the oxygen concentration outside this layer equals the bulk concentration and therefore, there is no concentration gradient along the $x$-axis. At last, the macroporous layer is made of black rust which is known to have a metallic electronic behavior. Thus with the present model, all the assumptions of the de Levie's theory are verified.

## 2.4. Regression

With the model illustrated in Fig. 3, the impedance diagrams were analyzed by using a non-linear least-squares regression procedure to extract physically meaningful parameters. The results of the regression are shown in Fig. 1 for 2 mg $l^{-1}$ of CL. Whatever the time of immersion, the model fits the experimental data very well.

In Fig. 4, the modulus of $\coth\left(l\sqrt{2\rho/rZ_{eq}}\right)$ was plotted in function of frequency for different times of immersion in Evian mineral water added with 2 mg $l^{-1}$ of CL. For 1 and 3 days of immersion, the impedance value obtained at the higher frequency differs from the electrolyte resistance (Fig. 1) and then $Z_0$ keeps a finite value; as a consequence, $\left|\coth\left(l\sqrt{2\rho/rZ_{eq}}\right)\right|$ always differs from 1. For 4 days of immersion, $\left|\coth\left(l\sqrt{2\rho/rZ_{eq}}\right)\right|$ differs from 1 only in the low frequency domain, which means that for high frequencies, the macropores behave as though they were semi-infinitely deep. For 1, 3 and 4 days of immersion, the macropores have a finite length and $l$, $r$ and $n$ can be regressed from the experimental data. For longer times, $\left|\coth\left(l\sqrt{2\rho/rZ_{eq}}\right)\right|$ equals 1 whatever the frequency, which corresponds to semi-infinitely deep macropores. In this case, $r$ and $n$ cannot be determined separately, only the product ($r^{3/2}n$) can be regressed.

Display Full Size version of this image (7K)

Fig. 4. Modulus of $\coth\left(1\sqrt{2\rho/rZ_{eq}}\right)$ vs. frequency for cast iron in Evian mineral water added with 2 mg $l^{-1}$ of CL, in function of immersion time at $E_{corr}$ and 150 rpm.

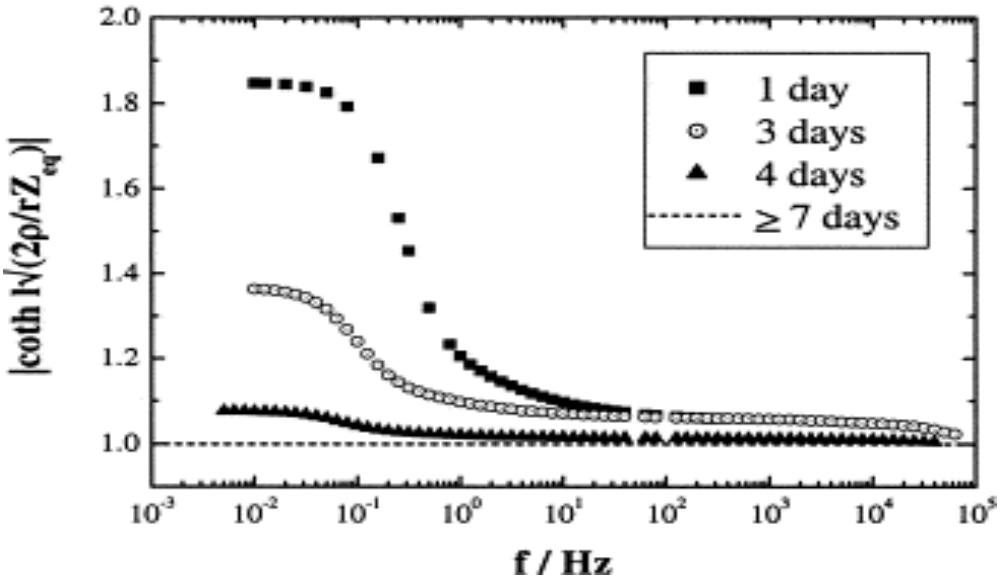


Moreover, it has been checked that $\coth\left(1\sqrt{2\rho/rZ_{eq}}\right)$ also differs from $\left(1\sqrt{2\rho/rZ_{eq}}\right)^{-1}$ for short times of immersion, which means that the cast iron–drinking water system does not respond like a plane interface. Thus, although impedance diagrams are not distorted in the so-called Warburg domain (angle of 45°), a regression of the data by a plane electrode model where $Z_c$ is directly proportional to $Z_0$, would not give satisfactory results. A porous electrode model is necessary to get a good adjustment, even at the first days of immersion, where no porous behavior is obvious.

## 2.5. Pore parameters

From the regression procedure, the mean length of the macropores, their radius and their number can be extracted. The corresponding values are presented in Table 1 and Fig. 5, in function of immersion time and CL concentration. In the present case, the length of the macropores corresponds to the thickness of the black rust layer.

Table 1. Corrosion of cast iron in drinking water

| Immersion time (day) | ℓ (μm) 1 | 2 | 3 | 4 | 7 | ≥10 | $n$ (cm$^{-2}$) |
|---|---|---|---|---|---|---|---|
| [*CL*] (*mg l*$^{-1}$) | | | | | | | |
| 0 | 150 | b | b | b | b | b | 12750 |
| 0.5 | a | a | a | 12 | 18 | b | 44650 |
| 2 | 16 | a | 25 | 54 | b | b | 44150 |

Mean length of the macropores ℓand number of macropores *n*, extracted from the regression procedure, vs. time of immersion and CL concentration.

Fig. 5. Radius of the macropores vs. time of immersion in Evian mineral water, for different CL concentrations. Cast iron electrode rotating at 150 rpm and $E_{corr}$.

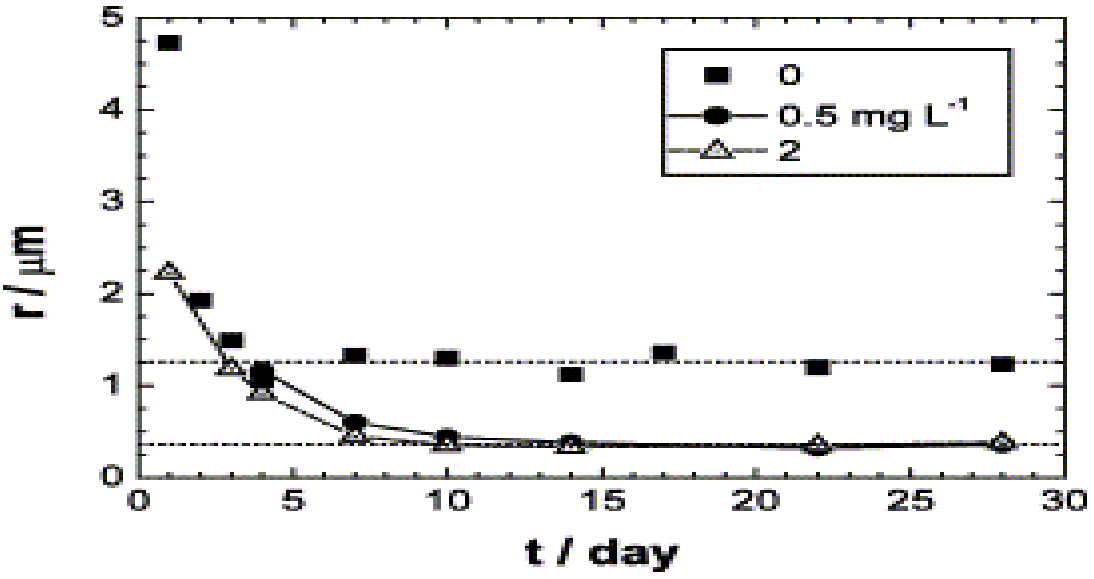


At short times of immersion, the layer of black rust is much thicker without CL (ℓ=150 μm) than with CL. Moreover, for high CL concentration, this macroporous layer is also thicker (ℓ =54 μm for 2 mg l$^{-1}$ of CL and ℓ=18 μm for 0.5 mg l$^{-1}$ of CL) and its growth kinetics is faster (ℓ is considered as semi-infinite after 7 days of immersion for 2 mg l$^{-1}$ of CL and after 10 days for 0.5 mg l$^{-1}$).

When the macropores can be considered as semi-infinitely deep, *r* and *n* are dependent parameters: only the product $r^{3/2}n$ can be regressed. Therefore, as soon as ℓ=∞, *n* is fixed and *r*

is calculated from $r^{3/2}n$. This fixed value for $n$ depends on the absence or the presence of CL but is similar for the two CL concentrations (see Table 1, last column).

For the chlorinated and non-chlorinated solutions, the radius of the macropores reach a stationary value as soon as the macropores can be considered as semi-infinitely deep (Fig. 5). Again this stationary value depends on the absence or the presence of CL but is similar for the two CL concentrations. Furthermore, macropores are wider without CL ($r$=1.25 μm) than with CL ($r$=0.35 μm).

Thus, without CL, the macropores are less numerous, longer and wider than with CL.

Obviously the kinetic parameters and the capacitances involved in the model are simultaneously obtained. The corresponding values, not presented here due to the aim of the present paper, are very close to those obtained in Ref. [14].

## 3. Electrodissolution of copper in 1 M hydrochloric acid solution

The anodic dissolution of copper in chloride medium has been widely studied in the literature [17, 18, 19, 20, 21, 22, 23, 24 and 25]. For neutral and acid chloride media, the impedance diagrams in the active dissolution region present two capacitive loops ( Fig. 6). These diagrams have been explained by the following mechanism:

$$Cu + Cl^- \underset{k_{-1}}{\overset{k_1}{\Leftrightarrow}} CuCl + e^- \quad (8)$$

$$CuCl + Cl^- \underset{k_{-2}}{\overset{k_2}{\Leftrightarrow}} CuCl_2^- \quad (9)$$

CuCl is an intermediary species adsorbed at the electrode surface and the steady-state current is partially controlled by mass transport of $CuCl_2^-$ [20].

Fig. 6. (●) Experimental and (□) regressed ac impedance diagrams of copper in 1 M HCl, plotted at −0.240 V vs. SCE and for two rotation speeds: (a) 100 and (b) 400 rpm. Some frequencies expressed in Hz are indicated on the diagrams.

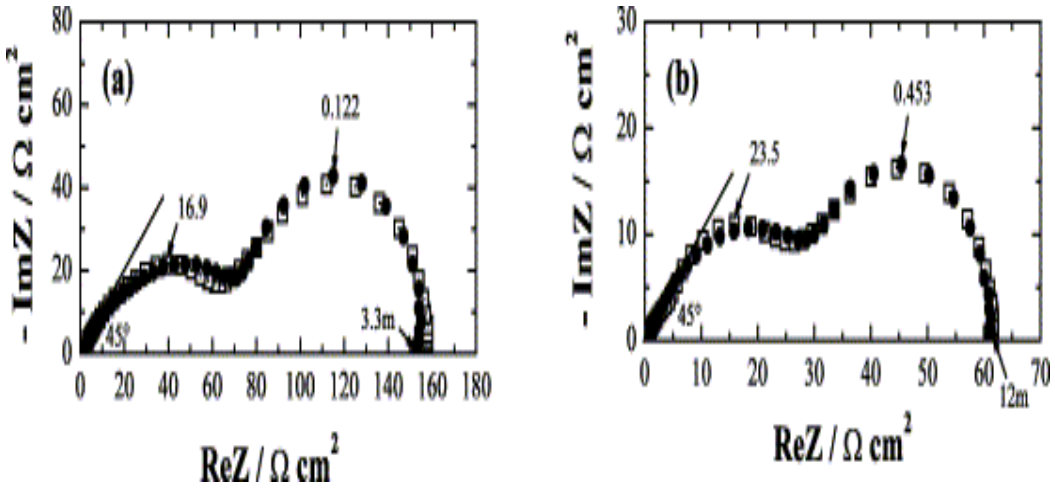


Although this mechanism can simulate the main results concerning the electrodissolution of copper in hydrochloric acid solution, it cannot explain the linear part observed in the very high frequency region with a slope of about 0.5 (Fig. 6) [25 and 26]. The following study will show how, by using the de Levie's theory described above, this linear behavior can be explained.

## 3.1. Experimental

All electrochemical measurements were performed with a three-electrode cell. The working electrode was a rotating disk electrode (RDE) consisting of a cylindrical pure copper rod with a 0.2 $cm^2$ cross-sectional area, the reference electrode was a saturated calomel electrode and the counter electrode was a large platinum grid. The solution was 1 M HCl (pH 0).

For electrochemical impedance measurements, a 1286 SOLARTRON potentiostat–galvanostat and a 1250 SOLARTRON Frequency Response Analyzer were used, with a frequency domain ranging from 65 kHz to a few mHz.

Due to the high renewal of the interface in the electrodissolution process, no ex situ surface analysis can be accurately performed. Therefore, no direct evidence of porous electrode was obtained.

## 3.2. Ac impedance model

Diard et al. [25] have proposed a physical model of the copper–HCl interface that can be represented by the equivalent circuit of Fig. 7. Thus, the impedance $Z_{eq}$ is modeled by the double layer capacitance $C_{dc}$, in parallel with the Faradaic impedance. The Faradaic impedance is given by the charge transfer resistance $R_t$ in series with an element calculated by taking into account the CuCl adsorption and the convective diffusion of $CuCl_2^-$. In Fig. 7, $C_{ads}$ is the adsorption capacitance, $R_{ads}$ the adsorption resistance and $Z_d$ a diffusion impedance described by:

Fig. 7. Ac impedance model for the copper–1 M HCl system, at −0.240 V vs. SCE. Equivalent circuit for the interfacial impedance per surface unit $Z_{eq}$ from Ref. [11].

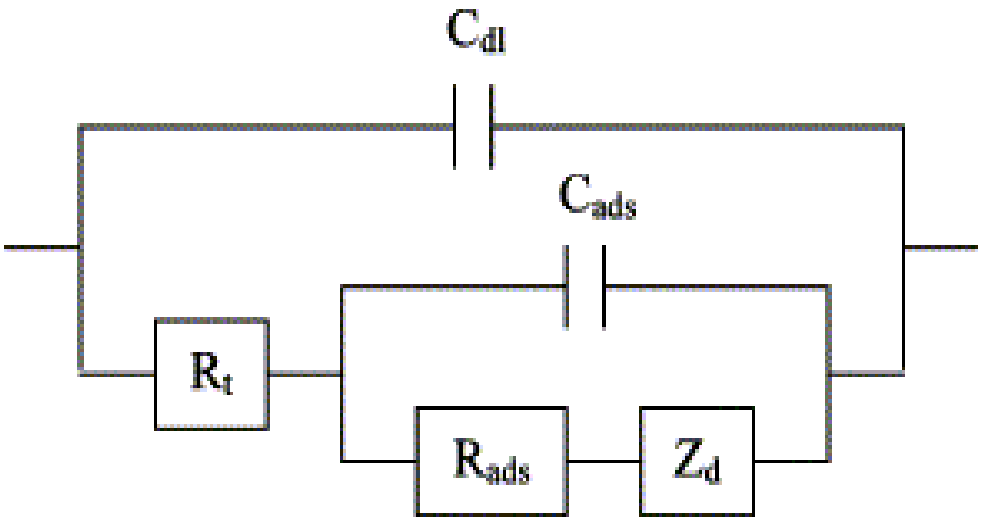


The general numerical solution developed in [27] was used for the calculation of $\left(-1/\theta'_{CuCl_2^-}(0)\right)$ at each frequency. This treatment takes into account the convective diffusion to the disk electrode with a finite Schmidt number, where the axial velocity is treated by a two-term expansion.

The experimental impedance is deduced from $Z_{eq}$ according to Eq. 5.

Given this kinetic model, an axial concentration gradient of $CuCl_2^-$ must exist, which is contrary to the de Levie's assumptions. However, $CuCl_2^-$ plays a role essentially in the diffusion impedance that is significant in the low frequency range where the electrode behavior is the closest to that of a plane electrode. For this reason, this porous electrode model can be used as a first approximation. Concerning the ohmic drop along the *x*-axis, it can be neglected due to the high conductivity of the solution.

### 3.3. Regression and pore parameters

The previous ac impedance model was used to regress the experimental impedance diagrams plotted at two different rotation speeds (Fig. 6). The results of the fitting are shown in Fig. 6. A very good match was obtained between the experimental results and the theoretical ones.

In Fig. 8, the modulus of $\coth\left(l\sqrt{2\rho/rZ_{eq}}\right)$ has been plotted in function of frequency for 100 rpm. $\left|\coth\left(l\sqrt{2\rho/rZ_{eq}}\right)\right|$ differs from 1 for frequencies lower than 100 Hz and equals 1 for higher frequencies. It means that above 100 Hz, the pores behave as though they were semi-infinitely deep. Moreover, it has been checked that $\left|\coth\left(l\sqrt{2\rho/rZ_{eq}}\right)\right|$ also differs from $\left(l\sqrt{2\rho/rZ_{eq}}\right)^{-1}$, which means that the electrochemical system does not respond like a plane electrode even in the very low frequency range.

Fig. 8. Modulus of $\coth\left(l\sqrt{2\rho/rZ_{eq}}\right)$ vs. frequency for the electrodissolution of copper in 1 M HCl. Potential, −0.240 V vs. SCE; and rotation speed, 100 rpm.

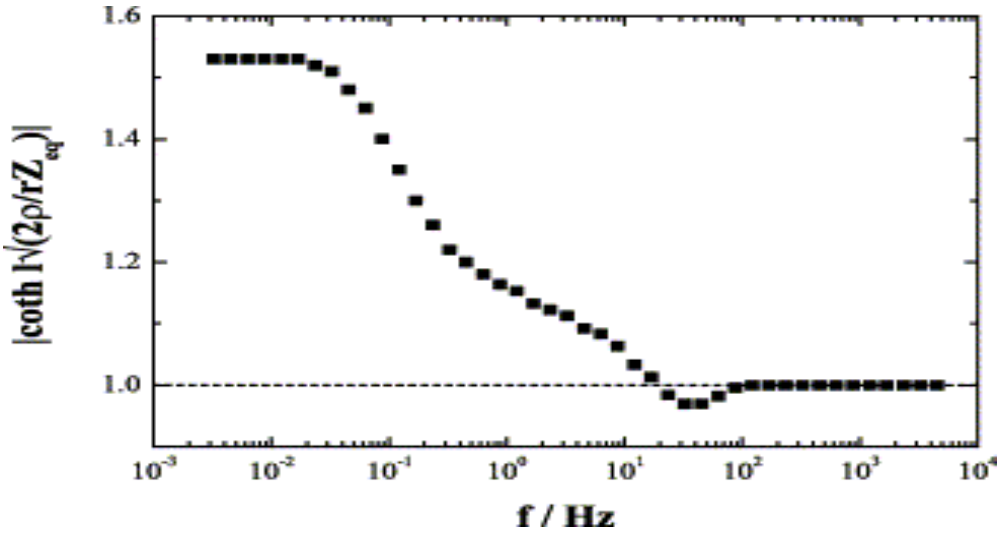

From the regression, values for the pore length ‡, the pore radius *r* and the number of pores *n* were obtained (Table 2). With increasing rotation speed, the pores become more numerous and shorter, but their radius remains identical. At 400 rpm, the pores are roughly twice as numerous and twice as short as at 100 rpm. As for the corrosion of cast iron, the kinetics parameters are simultaneously obtained.

Table 2. Electrodissolution of copper in 1 M hydrochloric acid solution

| Parameter | 100 rpm | 400 rpm |
|---|---|---|
| ‡ (μm) | 90 | 45 |
| *r* (μm) | 3.5 | 3.6 |
| *n* ($cm^{-2}$) | 6050 | 14 400 |

Mean length ‡, radius *r* and number *n* of the pores, extracted from the regression procedure, for two rotation speeds.

## 4. Conclusions

It was shown that the electrochemical impedance spectroscopy is a very useful tool for determining the characteristics of porous electrodes. Even for a very intricate pore geometry, the impedance can be represented by an equivalent cylindrical pore model. That is why de Levie's theory with cylindrical pores was used to fit experimental data of practical systems exhibiting a porous behavior. Mean values for the pore radius *r*, the pore length ‡ and the number of pores *n* were obtained if the pores were not semi infinite in the whole frequency range and for semi infinite pores, only the product $r^{3/2}n$ was regressed.

Even if the shape of the impedance diagrams suggests a plane electrode behavior, especially in the high frequency range, the electrochemical system can reveal porous electrode geometry. Therefore, in some cases where a plane electrode model does not give a good adjustment of experimental data, a porous electrode model should be used, as for example for the cast iron after 1 day of immersion (Fig. 1). Maybe porous electrode geometries are more frequent in the electrodissolution or in the corrosion field. This way could be used to analyze some problems where CPE are introduced without clear justification.

# References


B.A. Boukamp *Solid State Ionics* 20 (1986), p. 31.

R. de Levie *Adv. Electrochem. Electrochem. Eng.* 6 (1967), p. 329.

P. Los, A. Lasia, H. Ménard and L. Brossard *J. Electroanal. Chem.* 360 (1993), p. 101.

H. Keiser, K.D. Beccu and M.A. Gutjahr *Electrochim. Acta* 21 (1976), p. 539.

J.-P. Candy, P. Fouilloux, M. Keddam and H. Takenouti *Electrochim. Acta* 26 (1981), p. 1029.

J.-P. Candy, P. Fouilloux, M. Keddam and H. Takenouti *Electrochim. Acta* 27 (1982), p. 1585.

C. Hitz and A. Lasia *J. Electroanal. Chem.* 500 (2001), p. 213.

H.K. Song, Y.H. Jung, K.H. Lee and L.H. Dao *Electrochim. Acta* 44 (1999), p. 3513.

M. Keddam, C. Rakomotavo and H. Takenouti *J. Appl. Electrochem.* 14 (1984), p. 437.

C. Cachet and R. Wiart *J. Electroanal. Chem.* 195 (1985), p. 21.

A. Lasia *J. Electroanal. Chem.* 397 (1995), p. 27.

A. Lasia *J. Electroanal. Chem.* 428 (1997), p. 155.

L. Kiéné, W. Lu, Y. Levi, in: Proceeding A.W.W.A. W.Q.T.C., Boston, 1996.

I. Frateur, Thesis, University of Paris 6, France, 1997.

I. Frateur, C. Deslouis, M.E. Orazem and B. Tribollet *Electrochim. Acta* 44 (1999), p. 4345.

P. Drossbach and J. Schulz *Electrochim. Acta* 9 2 (1964), p. 1391.

A.L. Bacarella and J.C. Griess *J. Electrochem. Soc.* 120 (1973), p. 459.

M. Braun and K. Nobe *J. Electrochem. Soc.* 126 (1979), p. 1666.

A. Moreau, J.P. Frayret, F. Del Rey and R. Pointeau *J. Electrochem. Soc.* 27 (1982), p. 1281.

C. Deslouis, B. Tribollet, G. Mengoli and M. Musiani *J. Appl. Electrochem.* 18 (1988), p. 384.

A.K. Hauser and J. Newman *J. Electrochem. Soc.* 136 (1989), p. 3249.

F.K. Crundwell *Electrochim. Acta* 37 (1992), p. 2707.

O.E. Barcia, O.R. Mattos, N. Pébère and B. Tribollet *J. Electrochem. Soc.* 140 (1993), p. 2825.

J.-P. Diard, J.-M. Le Canut, B. Le Gorrec and C. Montella *Electrochim. Acta* 43 (1998), p. 2469.

J.-P. Diard, J.-M. Le Canut, B. Le Gorrec and C. Montella *Electrochim. Acta* 43 (1998), p. 2485.

J.B. Matos, E. D'Elia, O.E. Barcia, O.R. Mattos, N. Pébère and B. Tribollet *Electrochim. Acta* 46 (2001), p. 1377.

B. Tribollet and J. Newman *J. Electrochem. Soc.* 130 (1983), p. 2016.

Corresponding author. Tel.: +33-1-44276757; fax: +33-1-46340753; email: ifrateur@ext.jussieu.fr

Original text on Elsevier.com